ARTICLE

Apolipoprotein Mimetic Peptide Inhibits Neutrophil-Driven Inflammatory Damage via Membrane Remodeling and Suppression of Cell Lysis

Michelle W. Lee,[¶] Elizabeth Wei-Chia Luo,[¶] Carlos Silvestre-Roig,[¶] Yashes Srinivasan,[¶] Kiyotaka Akabori, Patricia Lemnitzer, Nathan W. Schmidt, Ghee Hwee Lai, Christian D. Santangelo, Oliver Soehnlein,* and Gerard C. L. Wong*

Cite This: https://doi.org/10.1021/acsnano.1c03978

Read Online

ACCESS | Metrics & More | Article Recommendations | Supporting Information

ABSTRACT: Neutrophils are crucial for host defense but are notorious for causing sterile inflammatory damage. Activated neutrophils in inflamed tissue can liberate histone H4, which was recently shown to perpetuate inflammation by permeating membranes via the generation of negative Gaussian curvature (NGC), leading to lytic cell death. Here, we show that it is possible to build peptides or proteins that cancel NGC in membranes and thereby suppress pore formation, and demonstrate that they can inhibit H4 membrane remodeling and thereby reduce histone H4-driven lytic cell death and resultant inflammation. As a demonstration of principle, we use apolipoprotein A-I (apoA-I) mimetic peptide apoMP$_1$. X-ray structural studies and theoretical calculations show that apoMP$_1$ induces nanoscopic positive Gaussian curvature (PGC), which interacts with the NGC induced by the N-terminus of histone H4 (H4n) to inhibit membrane permeation. Interestingly, we show that induction of PGC can inhibit membrane-permeating activity in general and "turn off" diverse membrane-permeating molecules besides H4n. *In vitro* experiments show an apoMP$_1$ dose-dependent rescue of H4 cytotoxicity. Using a mouse model, we show that tissue accumulation of neutrophils, release of neutrophil extracellular traps (NETs), and extracellular H4 all strongly correlate independently with local tissue cell death in multiple organs, but administration of apoMP$_1$ inhibits histone H4-mediated cytotoxicity and strongly prevents organ tissue damage.

KEYWORDS: *chronic inflammation, neutrophils, apolipoprotein, membrane remodeling, peptide—membrane interactions, cell death*

Histone H4n-induced pore   pore suppressed by apoMP$_1$
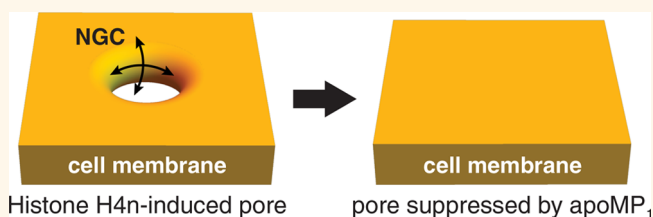
INTRODUCTION

Although neutrophils play important roles in host defense, they can also precipitate inflammation and tissue damage. Prolonged neutrophil infiltration stimulates inflammation and impedes its resolution.[1] Neutrophil activation triggers the release of inflammatory mediators such as cytokines, granule proteins, and neutrophil extracellular traps (NETs).[2] Excessive accumulation of such mediators promotes the destruction of the host tissue, resulting in nonresolving pathogenic inflammation. This pathogenic role of neutrophils is exemplified by multiple inflammatory pathologies including neurodegenerative diseases, obesity, arthritis, and sepsis.[1] Recent work indicates that proteins bound to NETs are involved in mediating neutrophil-associated damage. NETs are networks of extracellular fibers composed of DNA and externalized proteins of granule, cytoplasmic, and nuclear origin,[3] including histones, the release of which upon cell damage induces tissue

damage.[4,5] A machine-learning classifier[6] suggested that the N-terminus of histone H4 (H4n) has the capacity to generate negative Gaussian curvature (NGC) in lipid membranes,[3] a geometric requirement for membrane-permeating processes such as pore formation,[7] which can lead to cell death,[8] itself a potent pro-inflammatory signal. Small-angle X-ray scattering (SAXS) experiments confirmed these predictions.[3] Moreover, in hypercholesterolemic mouse models of atherosclerosis,[9] H4n induced lytic cell death in smooth muscle cells (SMCs),
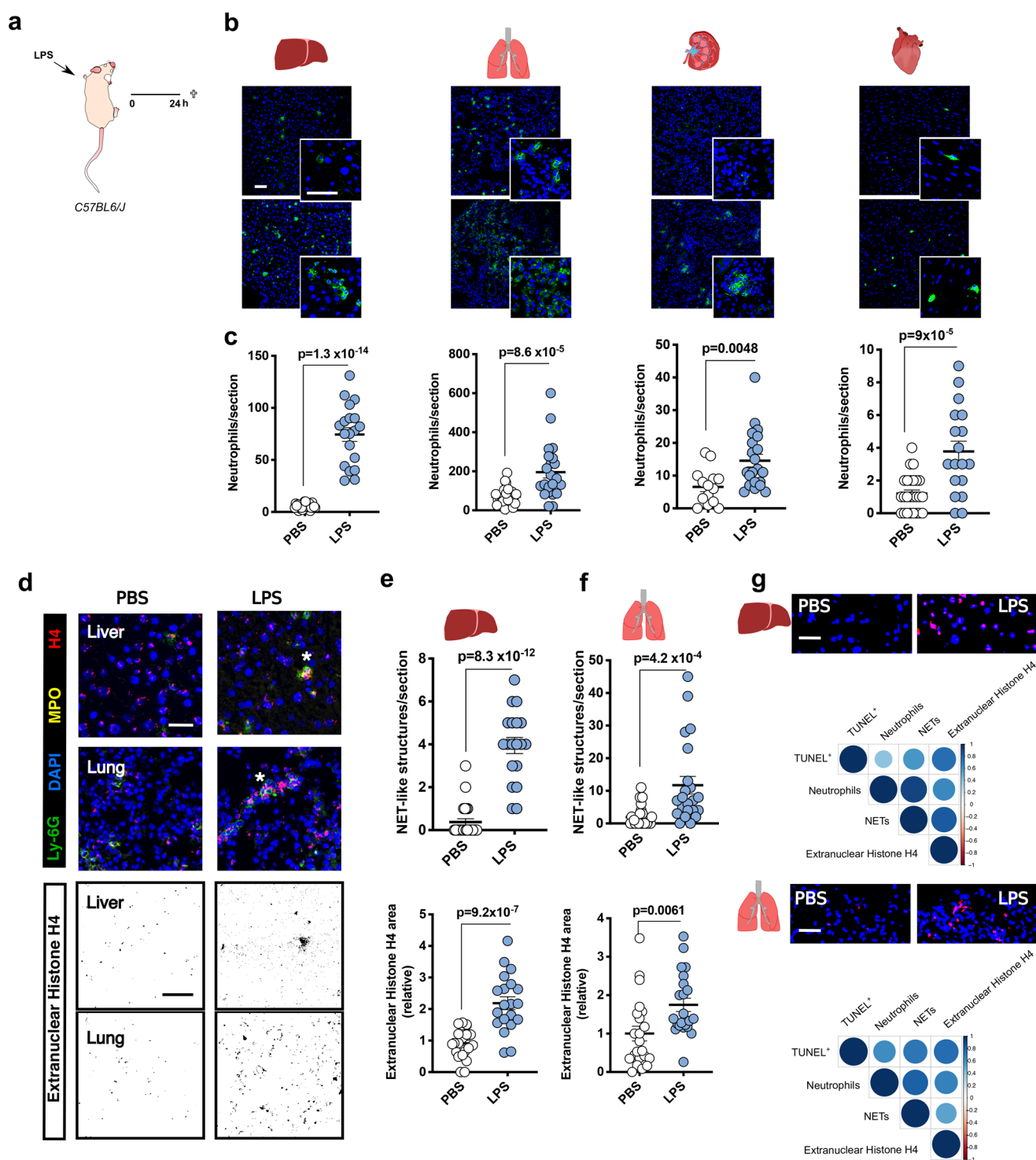
Figure 1. LPS-induced endotoxemia associates with multiorgan neutrophil infiltration, NET release, and tissue damage. (a–g) C57BL/6J mice were challenged with 10 mg/kg of LPS (*E. coli* O111:B4) or vehicle (PBS) for 24 h. (a) Schematic representation of the endotoxemia model. (b, c) From left to right, liver, lung, kidney, and heart. (b) Representative immunofluorescence micrographs showing tissue-infiltrated neutrophils (Ly6G, green) and nuclei (DAPI, blue) in indicated organs. Scale bar: 50 μm. (c) Quantification of infiltrated neutrophils in sections from indicated organs of PBS- or LPS-treated mice. n = 4−5 mice/group. (d) Representative immunofluorescence micrographs showing tissue NET-like structures (indicated with an asterisk) defined with the markers Ly6G, myeloperoxidase (MPO), histone H4, and DNA (DAPI), and extranuclear histone H4 in indicated organs. Extranuclear histone H4 is displayed as a binary image obtained from the subtraction of DAPI signal from histone H4 signal. Scale bar: 50 μm. Quantification of NETs (upper panel) and extranuclear histone H4 area (lower panel) in sections from liver (e) and lung (f) of PBS- or LPS-treated mice. n = 4−5 mice/group. (g) Representative immunofluorescence micrographs showing dead cells (TUNEL, red) and nuclei (DAPI, blue). Scale bar: 50 μm. Correlogram showing Pearson correlations between tissue TUNEL+ cells, neutrophil and NET numbers, and extranuclear histone H4 area in liver (upper panel) and lung (lower panel). n = 9−10 mice. Two-tailed t-test was used unless otherwise stated. All data is represented as mean ± SEM.

also consistent with machine learning and structural studies.[3] Clearly, regaining control of membrane permeation has important immunological consequences in suppressing runaway neutrophil-driven inflammation.

In this work, we show conceptually how peptides or proteins that induce positive Gaussian curvature (PGC, dome-shaped surface curvature) can suppress NGC (saddle-shaped surface curvature) and its consequences, including membrane permeation, lytic cell death, and associated organ damage from inflammation using a combination of synchrotron SAXS measurements, mean-field theory, *in vitro* cell studies, and *in vivo* animal studies. As a demonstration of principle, we use apoMP$_1$, a peptide mimic of apolipoprotein A-I (apoA-I), which is a protein that promotes PGC and organizes lipids into compact spherical high-density lipoprotein (HDL) particles for reverse cholesterol transport. Results from X-ray measurements and theoretical studies show that apoMP$_1$ induces nanoscopic PGC, which interacts with the NGC induced by H4n to inhibit NGC consequences such as membrane permeation. Consistent with this, *in vitro* experiments using murine endothelial cells, SMCs, macrophages, and hepatocytes show an apoMP$_1$ dose-dependent rescue of H4 cytotoxicity. Using a mouse model, we show that tissue accumulation of neutrophils, release of NETs, and extracellular H4 all strongly correlate independently with local tissue cell death in multiple organs, but administration of apoMP$_1$ inhibits histone H4-mediated cytotoxicity and strongly prevents organ tissue damage. These results exemplify a general mechanism for the suppression of membrane permeation that is mediated by membrane curvature rather than allosteric binding. The generality of these membrane-mediated interactions is highlighted with apoMP$_1$'s ability to "turn off" the membrane-remodeling activities of antimicrobial peptides (AMPs) and cell-penetrating peptides (CPPs), which are known to generate NGC in lipid membranes.[7,10−14] To show that these effects are not limited to apolipoprotein-like peptides and to validate this general concept of canceling out induced NGC by applying PGC, we design a peptide and demonstrate that it is also able to suppress the effects of membrane-disruptive peptides. Taken together, these results imply that histone-mediated cell death can be modulated with greater precision and resolution than previous thought possible through controlled membrane remodeling. More notably, the application of curvature as a means to nonspecifically inhibit membrane-remodeling events will help inform the development of therapeutics to treat conditions such as chronic inflammation.

The generation of NGC by pore-forming peptides is well-known.[7,10−12] To study the interaction between induced NGC and PGC in membranes, we need peptide sequences that (1) can generate nanoscopic positive curvature and (2) are soluble and able to freely exchange between different membranes. Lipoproteins are macromolecular complexes that consist of a hydrophobic core of neutral lipids, such as triglycerides and cholesteryl esters, surrounded by an outer layer of phospholipids, free cholesterol, and proteins. Lipoprotein particles are grouped into four major classes based on their density and size: chylomicrons, very low-density lipoproteins (VLDL), low-density lipoproteins (LDL), and HDL. Apolipoproteins, the protein component of lipoproteins, stabilize the geometric structure of lipoprotein particles as they undergo compositional modifications and are broadly classified into two groups, exchangeable (water-soluble) apolipoproteins, which can transfer between lipoprotein particles, and nonexchange-

able (water-insoluble) apolipoproteins, which remain bound to the same lipoprotein particle from biosynthesis to breakdown. The transport of lipids is typically facilitated by exchangeable apolipoproteins due to their ability to reversibly associate and dissociate from lipoproteins.[15−18] Exchangeable apolipoproteins are composed of multiple amphipathic α-helices,[19,20] which have been grouped into taxonomies based on their physicochemical properties.[15,21] While the distribution of different classes of amphipathic helices varies both within and among the different apolipoproteins and is believed to account for their diverse lipid affinities and functional properties,[22,23] details of how such helices enforce and maintain distinct lipoprotein structures are not known.

ApoA-I, an exchangeable apolipoprotein that contains 10 amphipathic α-helical segments, is the major protein constituent of HDL particles[24,25] and is central to HDL generation.[26] ApoA-I assembles and stabilizes lipids into spherical HDL species that are 7−12 nm in diameter.[24,27] When mixed, apoA-I and phospholipids are shown to spontaneously associate to form small micelle-like protein−lipid complexes.[15,28,29] Taken together, these findings suggest that the physicochemical properties and characteristics of apoA-I are conducive to the generation of PGC, although it is not clear *a priori* whether the quantitative amount of induced PGC is sufficient to turn off NGC needed for pore formation. Moreover, apoA-I being an exchangeable apolipoprotein allows for its diffusion and recycling between different cell membranes. Peptide analogs have been designed to mimic the lipid-associating helices of apoA-I.[30−34] Despite not having sequence homology to apoA-I, these mimetic peptides have individually been shown to recapitulate different aspects of apoA-I properties,[35−37] including, interestingly, some anti-inflammatory properties.[38] However, given the molecular differences between apoA-I and its peptide analogs and among the peptide analogs, the molecular basis of their therapeutic effects in dampening inflammation is not clear. On the basis of these considerations, we choose a well-characterized apoA-I mimetic peptide (apoMP) DWFKA-FYDKVAEKFKEAF[30,39] (D4F, which we refer to herein as apoMP$_1$ to emphasize its origin and functional role in self-assembly of compact spherical lipid particles).

RESULTS AND DISCUSSION

Uncontrolled inflammatory responses that occur during systemic inflammation can cause tissue destruction, multiorgan failure, and death.[40] Neutrophil hyperactivation in response to bacterial products triggers the release of NETs, the accumulation of which is associated with mortality during septicemia.[4] To interrogate the importance of NET-derived histone H4 on organ tissue damage during systemic inflammation, we administered lipopolysaccharide (LPS) from *E. coli* (O111:B4) intravenously in mice to mimic systemic Gram-negative bacterial infection (Figure 1a). LPS-induced endotoxemia associated with neutrophil activation and triggered multiorgan neutrophil infiltration (Figure 1b,c). In particular, in organs such as the lung and liver, which are especially vulnerable during endotoxemia, LPS infusion induced NET release and the accumulation of extranuclear histone H4 (Figure 1d−f), both of which were positively associated with increased tissue cell death (Figure 1g). Importantly, the levels of extranuclear histone H4 in the tissue positively correlated with the number of infiltrated neutrophils, hence suggesting that tissue histone H4 is of neutrophil origin.

Collectively, systemic activation of circulating neutrophils results in their entrapment in multiple tissues and the release of NET-derived histone H4 to cause tissue damage.

Using a mouse model of endotoxemia, we demonstrated that histone H4 molecules released during NETosis induce tissue damage and cell death in multiple organ systems. In previous studies, we showed that H4n can directly interact with cell membranes, remodel membrane curvature, and promote lytic cell death.[3] H4n consists of 24 amino acids, which include two α-helical segments in the α1 domain of the full histone H4 protein (Figure 2a). Its capacity to form membrane pores has
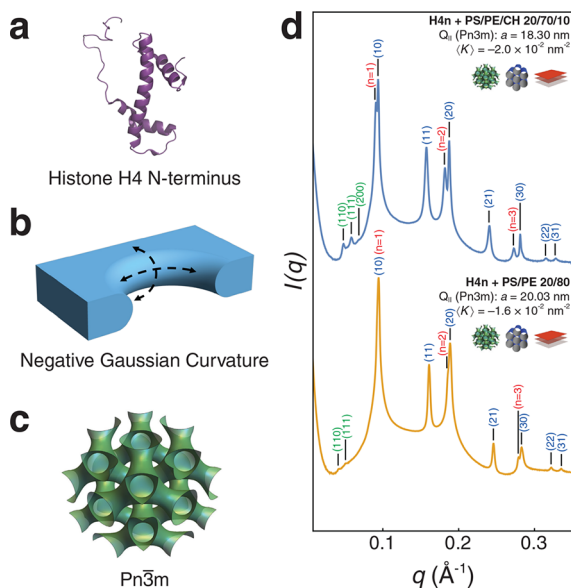

Figure 2. Histone H4 N-terminus induces stronger negative Gaussian curvature in cholesterol-rich membranes. (a) Rendering of H4n. (b) Model of NGC generation by H4n. (c) Representation of the Pn3m Q$_{II}$ phase. (d) SAXS spectra of H4n incubated with cholesterol-rich (PS/PE/CH 20/70/10) and cholesterol-poor (PS/PE 20/80) membranes at a P/L molar ratio of 1/40. H4n induces NGC in the form of a Pn3m Q$_{II}$ phase. Cholesterol enhances the membrane activity of H4n. Observed reflections for the cubic (green), hexagonal (blue), and lamellar (red) phases have been assigned on the spectra.

been attributed to the ability of its N-terminal domain to induce NGC in cell membranes, which is a geometric requirement for membrane-permeating events. Curvature at a point on a surface can be described by its principal curvatures, c_1 and c_2, along orthogonal axes. For a saddle-shaped deformation, the surface bends in opposite directions along these axes ($c_1 > 0$, $c_2 < 0$), resulting in a Gaussian curvature, $K \equiv c_1c_2$, that is negative (Figure 2b). These saddle-shaped surfaces are required to form the inner surface of a transmembrane pore and the bases of blebs.

Before assessing how apoMP$_1$ may influence the pore-forming activity of H4n, we conducted a control study to confirm H4n's ability to generate membrane-destabilizing curvature at lipid compositions of interest. Small unilamellar vesicles (SUVs) were prepared from ternary lipid mixtures of phosphatidylserine (PS), phosphatidylethanolamine (PE), and cholesterol (CH) at molar ratios of PS/PE 20/80 and PS/PE/CH 20/70/10. Because cholesterol constitutes a large fraction of mammalian cell membranes,[41] we used physiologically relevant cholesterol-containing SUVs to examine the effect of

cholesterol on the membrane-remodeling properties of H4n. For the model membrane PS/PE 20/80, we observed a coexistence of three phases: (1) a lamellar phase (L$_\alpha$) (peaks with q-ratios 1:2:3), (2) an inverse hexagonal phase (H$_{II}$) (peaks with q-ratios $\sqrt{1}:\sqrt{3}:\sqrt{4}:\sqrt{7}:\sqrt{9}:\sqrt{12}:\sqrt{13}$), and (3) a Pn3m inverse bicontinuous cubic phase (Q$_{II}$) with a lattice parameter of 20.03 nm (peaks with q-ratios $\sqrt{2}:\sqrt{3}:\sqrt{4}$) (Figure 2d). The Pn3m phase is rich in NGC (Figure 2c). For the cholesterol-containing model membrane PS/PE/CH 20/70/10, we again observed a similar phase coexistence but with a smaller lattice parameter in the Pn3m phase (18.30 nm) (Figure 2d, Table S1). In comparison, the control samples of PS/PE 20/80 SUVs only showed a broad feature of unilamellar vesicles and the control samples of PS/PE/CH 20/70/10 SUVs only exhibited an H$_{II}$ phase (Figure S1). To compare the Pn3m phases between cholesterol-rich and cholesterol-poor systems, we calculated the average amount of Gaussian curvature generated in each system using the equation $\langle K \rangle = 2\pi\chi/A_0a^2$, where a is the lattice parameter. The Euler characteristic, χ, and the surface area per unit cell, A_0, are specific for each cubic phase. For Pn3m, $\chi = -2$ and $A_0 = 1.919$. An increase in NGC magnitude from $\langle K \rangle = -1.6 \times 10^{-2}$ nm^{-2} for the PS/PE 20/80 membrane to $\langle K \rangle = -2.0 \times 10^{-2}$ nm^{-2} for the PS/PE/CH 20/70/10 membrane indicates that the presence of cholesterol promotes the ability of the H4n to generate membrane curvature. Interestingly, the magnitudes of NGC measured here are comparable with those generated by more hydrophobic AMPs with nonspecific activity against eukaryotic cells,[42] consistent with the contention of lytic cell death, and are within range of previous measurements for H4n.[3] Moreover, SAXS measurements indicate that H4n's ability to generate membrane-permeating curvature and lytic cell death increases with cholesterol content, which typically constitutes 30−40%[41] of mammalian cell membranes.

We hypothesized that apoMPs can interact with membranes in a manner that interferes with the membrane activity of histone H4 and, consequently, attenuate neutrophil-driven cytotoxicity and alleviate associated inflammation. We therefore investigated in detail the effect of apoMP$_1$ on NGC generation by H4n. We incubated PS/PE/CH 20/70/10 SUVs with H4n at a peptide-to-lipid (P/L) molar ratio of 1/40 and apoMP$_1$ at P/L molar ratios of 1/100, 1/50, and 1/25. SAXS measurements had shown that H4n alone induced correlation peaks characteristic of coexisting L$_\alpha$, H$_{II}$, and Pn3m Q$_{II}$ phases rich in NGC (Figure 2d). When coadministered with apoMP$_1$, however, the NGC-rich Pn3m cubic phases generated by H4n gradually disappeared with increasing concentration of apoMP$_1$ (Figure 3a, Table S1). These results imply that apoMP$_1$ can suppress effects associated with NGC generation (Figure 3e).

Interestingly, given that apolipoproteins are not known to bind histones, our results suggest that H4n and apoMP$_1$ interact with one another via a different mechanism rather than direct binding and allosteric inhibition. Since apoA-I assembles spheroidal HDL particles with small radii, it can stabilize positive membrane curvature by definition. Furthermore, deleting the helices that have the highest lipid affinities causes apoA-I to form larger particles, which have less positive curvature.[43] Consistent with that expectation, we find experimentally that apoMP$_1$ can transform an inverse hexagonal phase with strong negative mean curvature into a lamellar phase with zero mean curvature (Figure 3d). To test the idea that an apoMP may suppress H4n pore-forming activity via membrane-mediated interactions, we developed a
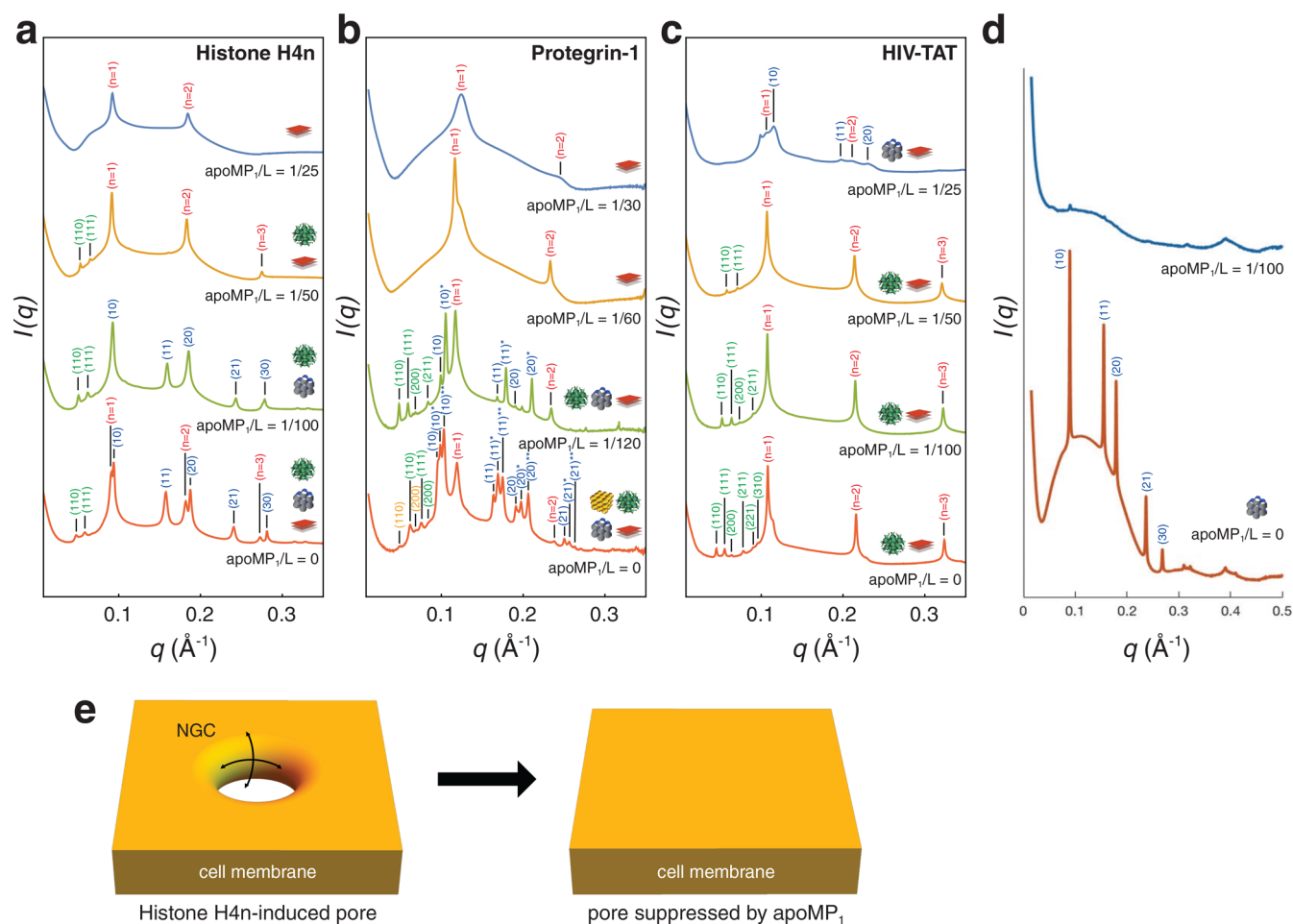
Figure 3. Apolipoprotein A-I mimic apoMP$_1$ inhibits the pro-lytic membrane activity of histone H4 N-terminus and unrelated peptides. (a) SAXS spectra of PS/PE/CH 20/70/10 SUVs incubated with H4n and apoMP$_1$. The P/L molar ratio of H4n was held constant at 1/40, while the P/L molar ratio of apoMP$_1$ was varied. H4n alone induced L$_\alpha$, H$_{II}$, and *Pn3m* Q$_{II}$ phases. *Pn3m* Q$_{II}$ phases were suppressed at high concentrations of apoMP$_1$. (b) SAXS spectra of PS/PE 20/80 SUVs cotreated with the AMP PG-1 (NGC-generating peptide) and apoMP$_1$. The P/L molar ratio of PG-1 was held constant at 1/40, while the P/L molar ratio of apoMP$_1$ was varied. PG-1 alone induced L$_\alpha$, H$_{II}$, *Pn3m* Q$_{II}$, and *Im3m* Q$_{II}$ phases. *Pn3m* and *Im3m* Q$_{II}$ phases were suppressed at high P/L molar ratios of apoMP$_1$, leaving behind a zero-curvature L$_\alpha$ phase. (c) SAXS spectra of PS/PE 20/80 SUVs cotreated with the CPP HIV-TAT (NGC-generating peptide) and apoMP$_1$. The P/L molar ratio of HIV-TAT was held constant at 1/40, while the P/L molar ratio of apoMP$_1$ was varied. HIV-TAT alone induced L$_\alpha$ and *Pn3m* Q$_{II}$ phases. *Pn3m* Q$_{II}$ phases were suppressed at high P/L molar ratios of apoMP$_1$, leaving behind L$_\alpha$ and H$_{II}$ phases. (d) ApoMP$_1$ can transform an H$_{II}$ phase with strong negative mean curvature into an L$_\alpha$ phase with zero mean curvature. (a–d) Observed reflections for the *Pn3m* cubic (green), *Im3m* cubic (yellow), hexagonal (blue), and lamellar (red) phases have been assigned on the curves. (e) Schematic portrayal of the suppression of H4n-induced NGC and pore formation by apoMP$_1$.

theoretical model (Supporting Information) for mixtures of two membrane-bound peptides (or proteins), one inducing negative (−) Gaussian curvature (e.g., saddle-shaped deformations from H4n) and the other inducing positive (+) Gaussian curvature (e.g., dome-shaped deformations from apoMP$_1$), in which positive curvature is induced in the membrane with no assumed preferred direction. Each peptide is taken to induce local principal curvatures in the membrane, ξ_1 and ξ_2, which work against the membrane deformations given by the Helfrich free energy over the membrane area $F_{\text{Helfrich}} = (\kappa/2)\int dA(c_1 + c_2)^2$ with bending rigidity κ. The energy of a single (±) peptide is $E_\pm / (k_B T) = (\lambda/2)[(c_1 - \xi_{1,\pm})^2 + (c_2 - \xi_{2,\pm})^2]$ when the peptide's maximal curvature is aligned with the membrane's, where $(\lambda/2)(\xi_{1,\pm}^2 + \xi_{2,\pm}^2)$ is the energy cost of binding a peptide to a flat membrane, λ is a dimensionless coupling constant, and

the induced principal curvatures depend on the peptide type. Analogous to classical nucleation theory, the free energy scales as $E = -\sigma\pi r^2 + 2\pi r\Gamma$ for a pore of radius r and pore rim line tension Γ on a membrane with effective surface tension σ. This model exhibits an energy barrier $E_{\text{barrier}} = \pi\Gamma^2/\sigma$ at a radius $r_0 = \Gamma/\sigma$. When this energy is comparable to thermal energy, pore formation becomes favorable. Mixtures of peptides inducing competing curvatures can control pore formation via this free energy barrier. We find that $K < 0$-inducing peptides, such as H4n, universally suppress the free energy barrier, while peptides that induce PGC ($K > 0$), such as apoMP$_1$, raise the barrier drastically even at modest area fractions (Figure 4a). The precise values used for constants do not change the generic behavior observed in the model. Additionally, the model predicts that the cubic phase lattice parameter a_{Pn3m} generally grows with increasing $K > 0$-inducing to $K < 0$-inducing peptide ratio (Figure 4b). (To see a summary of the interplay between Gaussian curvature, Gaussian modulus $\bar{\kappa}$,
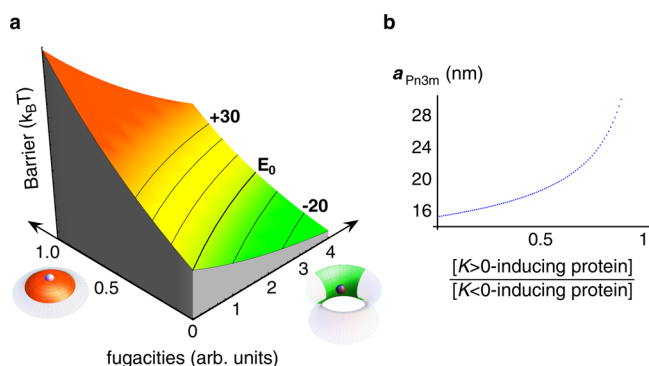
Figure 4. Positive Gaussian curvature induced by peptides can restrain pores formed by negative Gaussian curvature-inducing peptides: (a) Barrier height of pore formation for mixtures of $K > 0$-inducing (orange) and $K < 0$-inducing (green) peptides or proteins in theoretical model (Supporting Information). Barrier without proteins E_0 given by $E_0/k_BT = \pi\Gamma_0^2/\sigma_0$, with contours 10 k_BT apart. (b) Protein-prescribed curvatures mapped into corresponding equilibrium a_{Pn3m}, which grow with increasing molar ratio of $K > 0$-generating to $K < 0$-generating proteins, consistent with H4n/apoMP$_1$ experimental trends.

and the propensity for pore formation, we refer the interested reader to a recent review.[44])

The suppression mechanism of membrane permeation described by the above theoretical model does not require specific binding between the two types of peptides. To investigate the generality of apoMP$_1$-induced NGC suppression, we examined whether apoMP$_1$ could turn off NGC generated by amphiphilic peptides unrelated to histone-induced inflammation and with no sequence homology to histones, including the AMP protegrin-1 (PG-1) and the CPP human immunodeficiency virus type 1 trans-activator of transcription (HIV-TAT). PG-1 is an 18-amino acid β-hairpin structure[45] and possesses broad-spectrum antimicrobial activity against bacteria, fungi, and viruses[46] via membrane disruption.[47] We incubated PS/PE 20/80 SUVs with PG-1 at a P/L molar ratio of 1/40. PG-1 alone induced correlation peaks characteristic of coexisting L_α, H_{II}, $Pn3m$ Q_{II}, and $Im3m$ Q_{II} phases (Figure 3b, Table S1). ApoMP$_1$ exhibited dose-dependent suppression of the NGC induced by PG-1: apoMP$_1$ first suppressed the $Im3m$ phase at a P/L ratio of 1/120 before completely eliminating NGC, as evidenced by the absence of $Pn3m$ phase peaks at a P/L ratio of 1/60. Similarly, apoMP$_1$ suppresses NGC generated by the CPP HIV-TAT,[14] a protein that enhances viral transcription.[48] HIV-TAT alone at a P/L ratio of 1/40 remodeled PS/PE 20/80 SUVs into L_α and $Pn3m$ Q_{II} phases. In the presence of apoMP$_1$, at increasing P/L ratios from 1/100 to 1/25, NGC was again suppressed in a dose-dependent manner. At the
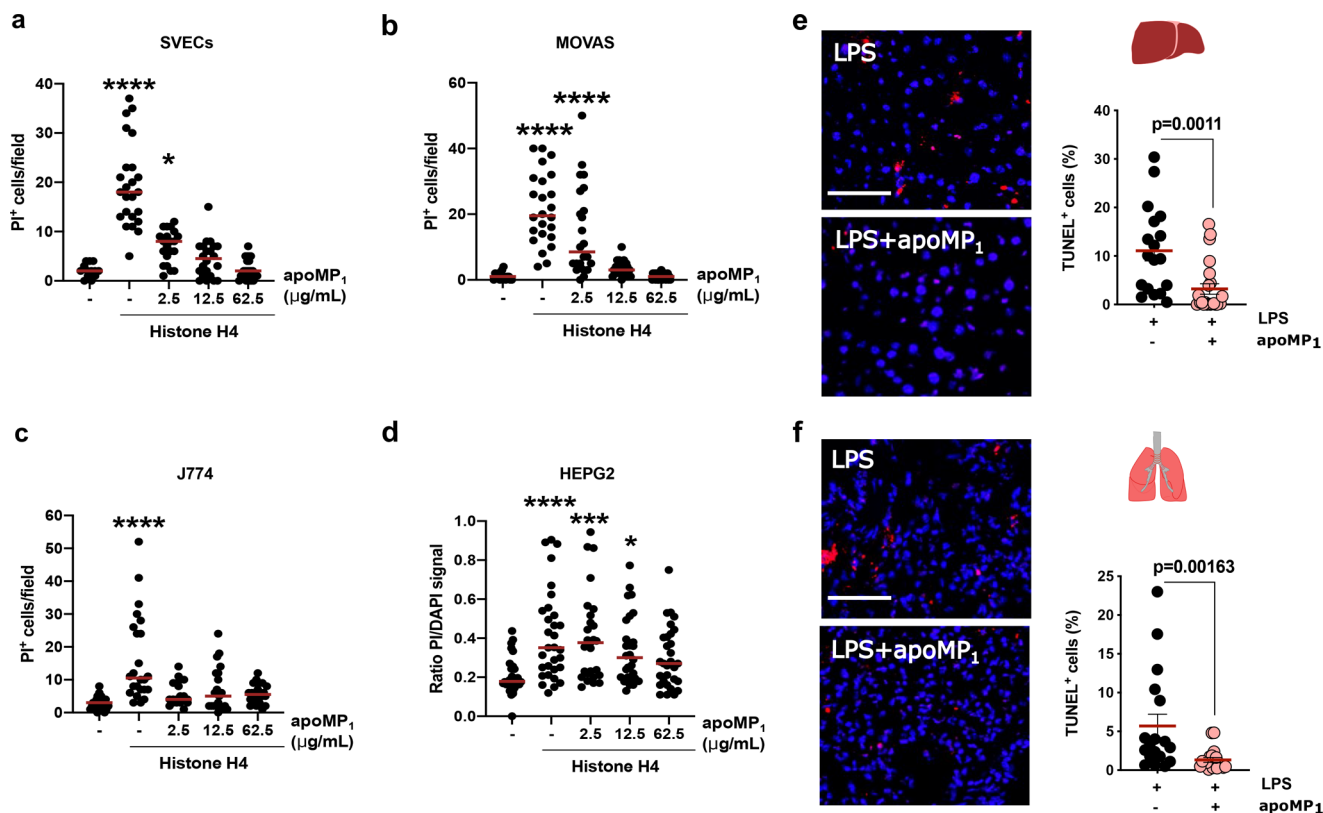

Figure 5. ApoMP$_1$ blocks histone H4-mediated cytotoxicity and prevents organ tissue damage after LPS-induced endotoxemia. (a−d) Histone H4-induced cell death quantified by PI uptake in murine endothelial cells (a), smooth muscle cells (b), macrophages (c), and hepatocytes (d) treated with indicated doses of apoMP$_1$. $n = 13-31$ fields. Results obtained from three independent experiments. One-way ANOVA with Dunnett's correction. *, $p < 0.05$; ***, $p < 0.001$; ****, $p < 0.0001$. (e, f) C57BL/6J mice were challenged with 10 mg/kg of LPS (*E. coli* O111:B4) for 24 h and treated with apoMP$_1$ (250 μg/intraperitoneal) or vehicle (saline). Representative immunofluorescence micrographs showing TUNEL$^+$ cells and quantification of percentage of TUNEL$^+$ cells in liver (e) and lung (f). Scale bar: 50 μm. $n = 5$ mice/group. Two-tailed t-test. All data is represented as mean $\pm$ SEM.

highest P/L ratio for apoMP$_1$, the system showed a complete absence of NGC-rich cubic phases (Figure 3c, Table S1). Clearly, apoMP$_1$ was able to suppress NGC generation, not just for H4n, but across disparate membrane-remodeling amphiphilic peptides that span AMPs and CPPs, which are drastically different from H4n in sequence, charge, and hydrophobicity. Certainly, it is possible for pore inhibition to involve direct binding between a pore-inhibiting peptide (or protein) and a pore-forming peptide (or protein),[49] based on their individual attributes. However, the results here demonstrating that a single peptide can suppress the effects of multiple pore-forming peptides indicate that direct binding is not required to inhibit the activity of a pore former and thus suggests that a general, nonspecific mechanism exists in parallel. In fact, the generality of these interactions mediated by induced membrane curvature can be seen in extant work on apoMPs: Despite their sequence diversity and lack of sequence homology to apoA-I, a vast number of apoMPs have successfully recapitulated many of the biological functions of apoA-I by mimicking its physicochemical and structural properties. To emphasize this point and the potential to multiplex different functions into these PGC-generating peptide sequences, we designed an antipore peptide APP-2498 that primarily uses arginine residues for its positively charged residues. In contrast, nearly all studied apoMPs exclusively utilize lysine in their positively charged residue positions.[22,31,33,34,39,50−52] We demonstrate that APP-2498 is capable of similar NGC suppression as apoMP$_1$ (Table S2, Figure S2). Indeed, we expect the existence of a general design architecture for antipore peptides.

SAXS measurements indicate that in the presence of apoMP$_1$, the generation of NGC by H4n is greatly attenuated, suggesting that the peptide is able to inhibit membrane-lytic cell death. Consistent with these observations, apoMP$_1$ was able to strongly inhibit the toxic capacity of H4n in different cell types in a dose-dependent fashion (Figure 5a−d). These effects were pronounced in endothelial cells, smooth muscle cells, and macrophages, while minor, yet significant, for hepatocytes. Next, to explore the therapeutic ability of apoMP$_1$ to prevent histone H4-mediated tissue damage, we treated mice with a single dose of apoMP$_1$ together with LPS administration. Notably, apoMP$_1$ treatment fully abrogated liver (Figure 5e) and lung (Figure 5f) tissue damage caused by LPS-induced hyperinflammation. Overall, our results support a host-tissue protective function of apoA-I through the prevention of NGC generation by neutrophil-derived histone H4.

Placing our results in a broader context, existing studies have shown that administration of either HDL or its primary protein component, apoA-I, exhibit anti-inflammatory and protective effects, including the reduction of atherosclerosis,[53] sepsis,[54,55] tumor growth,[56] macrophage activation,[57] and pro-inflammatory cytokine production.[58] However, due to the high dosages of apoA-I needed to achieve these effects, the design of smaller synthetic peptides to recapitulate the activities of apoA-I has recently attracted attention.[59,60] Both animal and human studies have shown that administration of these mimetic peptides leads to similar anti-inflammatory effects, which can treat conditions such as renal[61] and hepatic[62] inflammation, insulin resistance and diabetes,[36] arthritis,[63] asthma,[64] acute vascular inflammation,[31] and atherosclerosis.[30,33,35,65−68] Despite the ability of these mimetic designs to replicate the activities of HDL and apoA-I, the detailed mechanisms of their shared anti-inflammatory activities have been unclear. The findings presented here now suggest that inhibition of NGC generation in membranes by apoA-I and its mimics may explain some their observed anti-inflammatory effects.

CONCLUSIONS

A major challenge in modern medicine is discovering effective therapeutic strategies to inhibit cell death associated with inflammation, which impacts tissue function even after resolution of the acute inflammatory event. We show that LPS-induced sepsis causes neutrophil hyperactivation and release of NETs containing externalized nuclear proteins, including histone H4. Results here indicate that H4n induces rapid, receptor-independent cell death in multiple organs by generating NGC in cell membranes and forming membrane pores, in a manner that is promoted by cholesterol. Importantly, our findings suggest that an apoA-I mimetic peptide has the capacity to suppress histone-induced pore formation and cell death, and thereby prevent systematic tissue damage, through a membrane-mediated mechanism that is independent from direct protein−protein interactions. Our findings here showing that peptides that can suppress NGC have the ability to prevent systemic tissue and organ damage thus carry significant implications for the treatment of a broad range of inflammatory conditions.

METHODS/EXPERIMENTAL SECTION

Complete details of the experimental materials and methods are provided in the Supporting Information.

Peptides. Peptide apoMP$_1$ was a gift from Srinivasa T. Reddy and Alan M. Fogelman. All other peptides were synthesized by LifeTein using solid-phase synthesis or purchased from Anaspec.

SAXS Experiments. Lyophilized phospholipids were purchased from Avanti Polar Lipids and dissolved in chloroform as individual stock solutions. Lipid mixtures were prepared by combining the lipid stock solutions at the desired molar ratios and subsequently evaporated under nitrogen and desiccated overnight. The resulting dry lipid films were resuspended in aqueous buffer solution and incubated overnight at 37 °C. Lipid suspensions were sonicated until clear and extruded through a 0.2 μm pore filter to form SUVs. SUVs were mixed with peptides at specified P/L molar ratios and characterized using SAXS at the Stanford Synchrotron Radiation Lightsource (SSRL) and the Advanced Light Source (ALS).

Animal Experiments. All mouse experiments were carried out according to the European guidelines for the care and use of laboratory animals. Protocols were approved by the Committee on the Ethics of Animal Experiments of the Regierung von Oberbayern. For the mouse endotoxemia model, C57BL/6J mice were challenged with 10 mg/kg LPS from *E. coli* (O111:B4) and treated with 250 μg of apoMP$_1$ intraperitoneally or saline as control. Mice were sacrificed after 24 h, and lung, liver, kidney, and heart tissues were isolated and processed. Immunofluorescence staining was carried out on fixed cryosections and imaged using confocal microscopy.

Cell Viability Assays. Mouse vascular aorta/smooth muscle cells (MOVAS), J774A.1 macrophages, SVEC4-10 endothelial cells, and HepG2 human hepatocytes were incubated with 50 μg/mL histone H4 (Biomol) and specified amounts of apoMP$_1$. Cell viability was determined by propidium iodide (PI) uptake.

Statistics. Statistical analysis was carried out via GraphPad Prism 7 (GraphPad Software). The ROUT outlier function was used to exclude statistical outliers (Q = 1%). Normal distribution of the data was assessed using the D'Agostino-Pearson omnibus test for normality. Normally distributed data was tested by two-tailed unpaired *t*-test (one variable) or one-way ANOVA with Tukey's or Dunnet's correction (>2 variables). When 2 factors were analyzed, data was analyzed using two-way ANOVA with Tukey's correction. In

all tests a 95% confidence interval was used, with which $p < 0.05$ was considered a significant difference. Correlograms were generated using R. All data is represented as mean ± SEM.

ASSOCIATED CONTENT

Supporting Information

The Supporting Information is available free of charge at https://pubs.acs.org/doi/10.1021/acsnano.1c03978.

Full experimental materials and methods; symmetries, lattice parameters, and NGC values of induced cubic phases; SAXS spectra of control samples, SAXS spectra of membranes treated with NGC-generating peptides and APP-2498, schematic of a single peptide interacting with a curved membrane, and schematic of membrane-bound peptides in a model membrane pore (PDF)

AUTHOR INFORMATION

Corresponding Authors

Oliver Soehnlein − Institute of Experimental Pathology, Center for Molecular Biology of Inflammation (ZMBE), University of Münster, 48149 Münster, Germany; Department of Physiology and Pharmacology (FyFa), Karolinska Institute, 171 77 Stockholm, Sweden; Institute for Cardiovascular Prevention (IPEK), LMU Munich, 80336 Munich, Germany; Phone: +49 251 83-53064; Email: soehnlein@uni-muenster.de

Gerard C. L. Wong − Department of Bioengineering, University of California, Los Angeles, California 90095, United States; orcid.org/0000-0003-0893-6383; Phone: (310) 794-7684; Email: gclwong@seas.ucla.edu

Authors

Michelle W. Lee − Department of Bioengineering, University of California, Los Angeles, California 90095, United States; orcid.org/0000-0003-1613-9501

Elizabeth Wei-Chia Luo − Department of Bioengineering, University of California, Los Angeles, California 90095, United States; orcid.org/0000-0002-8663-0446

Carlos Silvestre-Roig − Institute of Experimental Pathology, Center for Molecular Biology of Inflammation (ZMBE), University of Münster, 48149 Münster, Germany; Institute for Cardiovascular Prevention (IPEK), LMU Munich, 80336 Munich, Germany

Yashes Srinivasan − Department of Bioengineering, University of California, Los Angeles, California 90095, United States; orcid.org/0000-0002-5279-9753

Kiyotaka Akabori − Department of Physics, University of Massachusetts, Amherst, Massachusetts 01003, United States

Patricia Lemnitzer − Institute of Experimental Pathology, Center for Molecular Biology of Inflammation (ZMBE), University of Münster, 48149 Münster, Germany

Nathan W. Schmidt − Department of Bioengineering, University of California, Los Angeles, California 90095, United States; Ginkgo Bioworks, Boston, Massachusetts 02210, United States

Ghee Hwee Lai − Department of Bioengineering, University of California, Los Angeles, California 90095, United States; Singapore Centre for Environmental Life Sciences Engineering (SCELSE), Nanyang Technological University, Singapore 637551

Christian D. Santangelo − Department of Physics, University of Massachusetts, Amherst, Massachusetts 01003, United States; Department of Physics, Syracuse University, Syracuse, New York 13244, United States

Complete contact information is available at:
https://pubs.acs.org/10.1021/acsnano.1c03978

Author Contributions

¶M.W.L., E.W.C.L., C.S.R., and Y.S. contributed equally to this work. Authorship order among co-first authors was determined alphabetically. M.W.L., E.W.C.L., C.S.R., Y.S., O.S., and G.C.L.W. designed the research. O.S. and G.C.L.W. supervised the research. M.W.L., E.W.C.L., C.S.R., Y.S., O.S., and G.C.L.W. wrote the manuscript. M.W.L., E.W.C.L., and Y.S. conducted synchrotron SAXS experiments and analyzed data. C.S.R. and P.L. conducted mouse experiments, cell culture experiments, immunofluorescence, and analyzed data. K.A. and C.D.S. developed the theoretical model for membrane curvature canceling. N.W.S. and G.H.L. carried out preliminary experiments and analysis. All authors reviewed and approved the final version of the manuscript.

Notes

The authors declare the following competing financial interest(s): A provisional patent application has been filed based on this work.

REFERENCES

(1) Soehnlein, O.; Steffens, S.; Hidalgo, A.; Weber, C. Neutrophils As Protagonists and Targets in Chronic Inflammation. *Nat. Rev. Immunol.* **2017**, *17*, 248−261.

(2) Papayannopoulos, V. Neutrophil Extracellular Traps in Immunity and Disease. *Nat. Rev. Immunol.* **2018**, *18*, 134−147.

(3) Silvestre-Roig, C.; Braster, Q.; Wichapong, K.; Lee, E. Y.; Teulon, J. M.; Berrebeh, N.; Winter, J.; Adrover, J. M.; Santos, G. S.; Froese, A.; Lemnitzer, P.; Ortega-Gómez, A.; Chevre, R.; Marschner, J.; Schumski, A.; Winter, C.; Perez-Olivares, L.; Pan, C.; Paulin, N.;

Schoufour, T.; et al. Externalized Histone H4 Orchestrates Chronic Inflammation by Inducing Lytic Cell Death. *Nature* **2019**, *569*, 236−240.

(4) Xu, J.; Zhang, X.; Pelayo, R.; Monestier, M.; Ammollo, C. T.; Semeraro, F.; Taylor, F. B.; Esmon, N. L.; Lupu, F.; Esmon, C. T. Extracellular Histones Are Major Mediators of Death in Sepsis. *Nat. Med.* **2009**, *15*, 1318−1321.

(5) Saffarzadeh, M.; Juenemann, C.; Queisser, M. A.; Lochnit, G.; Barreto, G.; Galuska, S. P.; Lohmeyer, J.; Preissner, K. T. Neutrophil Extracellular Traps Directly Induce Epithelial and Endothelial Cell Death: A Predominant Role of Histones. *PLoS One* **2012**, *7*, No. e32366.

(6) Lee, E. Y.; Fulan, B. M.; Wong, G. C. L.; Ferguson, A. L. Mapping Membrane Activity in Undiscovered Peptide Sequence Space Using Machine Learning. *Proc. Natl. Acad. Sci. U. S. A.* **2016**, *113*, 13588−13593.

(7) Schmidt, N. W.; Mishra, A.; Lai, G. H.; Davis, M.; Sanders, L. K.; Tran, D.; Garcia, A.; Tai, K. P.; McCray, P. B.; Ouellette, A. J.; Selsted, M. E.; Wong, G. C. L. Criterion for Amino Acid Composition of Defensins and Antimicrobial Peptides Based on Geometry of Membrane Destabilization. *J. Am. Chem. Soc.* **2011**, *133*, 6720−6727.

(8) Dathe, M.; Wieprecht, T. Structural Features of Helical Antimicrobial Peptides: Their Potential to Modulate Activity on Model Membranes and Biological Cells. *Biochim. Biophys. Acta, Biomembr.* **1999**, *1462*, 71−87.

(9) Silvestre-Roig, C.; de Winther, M. P.; Weber, C.; Daemen, M. J.; Lutgens, E.; Soehnlein, O. Atherosclerotic Plaque Destabilization. *Circ. Res.* **2014**, *114*, 214−226.

(10) Hickel, A.; Danner-Pongratz, S.; Amenitsch, H.; Degovics, G.; Rappolt, M.; Lohner, K.; Pabst, G. Influence of Antimicrobial Peptides on the Formation of Nonlamellar Lipid Mesophases. *Biochim. Biophys. Acta, Biomembr.* **2008**, *1778*, 2325−2333.

(11) Prenner, E. J.; Lewis, R. N. A. H.; Neuman, K. C.; Gruner, S. M.; Kondejewski, L. H.; Hodges, R. S.; McElhaney, R. N. Nonlamellar Phases Induced by the Interaction of Gramicidin S with Lipid Bilayers. A Possible Relationship to Membrane-Disrupting Activity. *Biochemistry* **1997**, *36*, 7906−7916.

(12) Keller, S. L.; Gruner, S. M.; Gawrisch, K. Small Concentrations of Alamethicin Induce a Cubic Phase in Bulk Phosphatidylethanolamine Mixtures. *Biochim. Biophys. Acta, Biomembr.* **1996**, *1278*, 241−246.

(13) Schmidt, N.; Mishra, A.; Lai, G. H.; Wong, G. C. L. Arginine-Rich Cell-Penetrating Peptides. *FEBS Lett.* **2010**, *584*, 1806−1813.

(14) Mishra, A.; Lai, G. H.; Schmidt, N. W.; Sun, V. Z.; Rodriguez, A. R.; Tong, R.; Tang, L.; Cheng, J.; Deming, T. J.; Kamei, D. T.; Wong, G. C. L. Translocation of HIV TAT Peptide and Analogues Induced by Multiplexed Membrane and Cytoskeletal Interactions. *Proc. Natl. Acad. Sci. U. S. A.* **2011**, *108*, 16883−16888.

(15) Segrest, J. P.; Jones, M. K.; De Loof, H.; Brouillette, C. G.; Venkatachalapathi, Y. V.; Anantharamaiah, G. M. The Amphipathic Helix in the Exchangeable Apolipoproteins: A Review of Secondary Structure and Function. *J. Lipid Res.* **1992**, *33*, 141−166.

(16) Remaley, A. T.; Schumacher, U. K.; Stonik, J. A.; Farsi, B. D.; Nazih, H.; Brewer, H. B. Decreased Reverse Cholesterol Transport from Tangier Disease Fibroblasts. *Arterioscler., Thromb., Vasc. Biol.* **1997**, *17*, 1813−1821.

(17) Remaley, A. T.; Stonik, J. A.; Demosky, S. J.; Neufeld, E. B.; Bocharov, A. V.; Vishnyakova, T. G.; Eggerman, T. L.; Patterson, A. P.; Duverger, N. J.; Santamarina-Fojo, S.; Brewer, H. B. Apolipoprotein Specificity for Lipid Efflux by the Human ABCAI Transporter. *Biochem. Biophys. Res. Commun.* **2001**, *280*, 818−823.

(18) Smith, L. E.; Segrest, J. P.; Davidson, W. S. Helical Domains That Mediate Lipid Solubilization and ABCA1-Specific Cholesterol Efflux in Apolipoproteins C-I and A-II. *J. Lipid Res.* **2013**, *54*, 1939−1948.

(19) McLachlan, A. D. Repeated Helical Pattern in Apolipoprotein-A-I. *Nature* **1977**, *267*, 465−466.

(20) Li, W. H.; Tanimura, M.; Luo, C. C.; Datta, S.; Chan, L. The Apolipoprotein Multigene Family: Biosynthesis, Structure, Structure−Function Relationships, and Evolution. *J. Lipid Res.* **1988**, *29*, 245−271.

(21) Segrest, J. P.; De Loof, H.; Dohlman, J. G.; Brouillette, C. G.; Anantharamaiah, G. M. Amphipathic Helix Motif: Classes and Properties. *Proteins: Struct., Funct., Genet.* **1990**, *8*, 103−117.

(22) Mishra, V. K.; Palgunachari, M. N. Interaction of Model Class A1, Class A2, and Class Y Amphipathic Helical Peptides with Membranes. *Biochemistry* **1996**, *35*, 11210−11220.

(23) Saito, H.; Lund-Katz, S.; Phillips, M. C. Contributions of Domain Structure and Lipid Interaction to the Functionality of Exchangeable Human Apolipoproteins. *Prog. Lipid Res.* **2004**, *43*, 350−380.

(24) Davidson, W. S.; Thompson, T. B. The Structure of Apolipoprotein A-I in High Density Lipoproteins. *J. Biol. Chem.* **2007**, *282*, 22249−22253.

(25) Kontush, A.; Chapman, M. J. *High-Density Lipoproteins: Structure, Metabolism, Function, and Therapeutics*; John Wiley & Sons, Inc.: Hoboken, NJ, 2011; p 648.

(26) Mishra, V. K.; Palgunachari, M. N.; Datta, G.; Phillips, M. C.; Lund-Katz, S.; Adeyeye, S. O.; Segrest, J. P.; Anantharamaiah, G. M. Studies of Synthetic Peptides of Human Apolipoprotein A-I Containing Tandem Amphipathic *α*-Helixes. *Biochemistry* **1998**, *37*, 10313−10324.

(27) Silva, R. A. G. D.; Huang, R.; Morris, J.; Fang, J.; Gracheva, E. O.; Ren, G.; Kontush, A.; Jerome, W. G.; Rye, K-A.; Davidson, W. S. Structure of Apolipoprotein A-I in Spherical High Density Lipoproteins of Different Sizes. *Proc. Natl. Acad. Sci. U. S. A.* **2008**, *105*, 12176−12181.

(28) Tall, A. R.; Small, D. M.; Shipley, G. G.; Lees, R. S. Apoprotein Stability and Lipid−Protein Interactions in Human Plasma High Density Lipoproteins. *Proc. Natl. Acad. Sci. U. S. A.* **1975**, *72*, 4940−4942.

(29) Atkinson, D.; Smith, H. M.; Dickson, J.; Austin, J. P. Interaction of Apoprotein from Porcine High-Density Lipoprotein with Dimyristoyl Lecithin. *Eur. J. Biochem.* **1976**, *64*, 541−547.

(30) Navab, M.; Anantharamaiah, G. M.; Reddy, S. T.; Hama, S.; Hough, G.; Grijalva, V. R.; Yu, N.; Ansell, B. J.; Datta, G.; Garber, D. W.; Fogelman, A. M. Apolipoprotein A-I Mimetic Peptides. *Arterioscler., Thromb., Vasc. Biol.* **2005**, *25*, 1325−1331.

(31) Di Bartolo, B. A.; Nicholls, S. J.; Bao, S.; Rye, K-A.; Heather, A. K.; Barter, P. J.; Bursill, C. The Apolipoprotein A-I Mimetic Peptide ETC-642 Exhibits Anti-Inflammatory Properties That Are Comparable to High Density Lipoproteins. *Atherosclerosis* **2011**, *217*, 395−400.

(32) Wool, G. D.; Reardon, C. A.; Getz, G. S. Apolipoprotein A-I Mimetic Peptide Helix Number and Helix Linker Influence Potentially Anti-Atherogenic Properties. *J. Lipid Res.* **2008**, *49*, 1268−1283.

(33) D'Souza, W.; Stonik, J. A.; Murphy, A.; Demosky, S. J.; Sethi, A. A.; Moore, X. L.; Chin-Dusting, J.; Remaley, A. T.; Sviridov, D. Structure/Function Relationships of Apolipoprotein A-I Mimetic Peptides. *Circ. Res.* **2010**, *107*, 217−227.

(34) Mendez, A. J.; Anantharamaiah, G. M.; Segrest, J. P.; Oram, J. F. Synthetic Amphipathic Helical Peptides That Mimic Apolipoprotein A-I in Clearing Cellular Cholesterol. *J. Clin. Invest.* **1994**, *94*, 1698−1705.

(35) Garber, D. W.; Datta, G.; Chaddha, M.; Palgunachari, M. N.; Hama, S. Y.; Navab, M.; Fogelman, A. M.; Segrest, J. P.; Anantharamaiah, G. M. A New Synthetic Class A Amphipathic Peptide Analogue Protects Mice from Diet-Induced Atherosclerosis. *J. Lipid Res.* **2001**, *42*, 545−552.

(36) Morgantini, C.; Imaizumi, S.; Grijalva, V.; Navab, M.; Fogelman, A. M.; Reddy, S. T. Apolipoprotein A-I Mimetic Peptides Prevent Atherosclerosis Development and Reduce Plaque Inflammation in a Murine Model of Diabetes. *Diabetes* **2010**, *59*, 3223−3228.

(37) Van Lenten, B. J.; Wagner, A. C.; Anantharamaiah, G. M.; Navab, M.; Reddy, S. T.; Buga, G. M.; Fogelman, A. M. Apolipoprotein A-I Mimetic Peptides. *Curr. Atheroscler. Rep.* **2009**, *11*, 52−57.

(38) Anantharamaiah, G. M.; Mishra, V. K.; Garber, D. W.; Datta, G.; Handattu, S. P.; Palgunachari, M. N.; Chaddha, M.; Navab, M.; Reddy, S. T.; Segrest, J. P.; Fogelman, A. M. Structural Requirements for Antioxidative and Anti-Inflammatory Properties of Apolipoprotein A-I Mimetic Peptides. *J. Lipid Res.* **2007**, *48*, 1915−1923.

(39) Datta, G.; Chaddha, M.; Hama, S.; Navab, M.; Fogelman, A. M.; Garber, D. W.; Mishra, V. K.; Epand, R. M.; Epand, R. F.; Lund-Katz, S.; Phillips, M. C.; Segrest, J. P.; Anantharamaiah, G. M. Effects of Increasing Hydrophobicity on the Physical-Chemical and Biological Properties of a Class A Amphipathic Helical Peptide. *J. Lipid Res.* **2001**, *42*, 1096−1104.

(40) Angus, D. C.; van der Poll, T. Severe Sepsis and Septic Shock. *N. Engl. J. Med.* **2013**, *369*, 840−851.

(41) Pinkwart, K.; Schneider, F.; Lukoseviciute, M.; Sauka-Spengler, T.; Lyman, E.; Eggeling, C.; Sezgin, E. Nanoscale Dynamics of Cholesterol in the Cell Membrane. *J. Biol. Chem.* **2019**, *294*, 12599−12609.

(42) Lee, M. W.; de Anda, J.; Kroll, C.; Bieniossek, C.; Bradley, K.; Amrein, K. E.; Wong, G. C. L. How Do Cyclic Antibiotics with Activity against Gram-Negative Bacteria Permeate Membranes? A Machine Learning Informed Experimental Study. *Biochim. Biophys. Acta, Biomembr.* **2020**, *1862*, 183302.

(43) Vedhachalam, C.; Chetty, P. S.; Nickel, M.; Dhanasekaran, P.; Lund-Katz, S.; Rothblat, G. H.; Phillips, M. C. Influence of Apolipoprotein (Apo) A-I Structure on Nascent High Density Lipoprotein (HDL) Particle Size Distribution. *J. Biol. Chem.* **2010**, *285*, 31965−31973.

(44) Schmidt, N. W.; Wong, G. C. L. Antimicrobial Peptides and Induced Membrane Curvature: Geometry, Coordination Chemistry, and Molecular Engineering. *Curr. Opin. Solid State Mater. Sci.* **2013**, *17*, 151−163.

(45) Steinberg, D. A.; Hurst, M. A.; Fujii, C. A.; Kung, A. H.; Ho, J. F.; Cheng, F. C.; Loury, D. J.; Fiddes, J. C. Protegrin-1: A Broad-Spectrum, Rapidly Microbicidal Peptide with *in Vivo* Activity. *Antimicrob. Agents Chemother.* **1997**, *41*, 1738−1742.

(46) Kokryakov, V. N.; Harwig, S. S. L.; Panyutich, E. A.; Shevchenko, A. A.; Aleshina, G. M.; Shamova, O. V.; Korneva, H. A.; Lehrer, R. I. Protegrins: Leukocyte Antimicrobial Peptides That Combine Features of Corticostatic Defensins and Tachyplesins. *FEBS Lett.* **1993**, *327*, 231−236.

(47) Lam, K. L. H.; Ishitsuka, Y.; Cheng, Y.; Chien, K.; Waring, A. J.; Lehrer, R. I.; Lee, K. Y. C. Mechanism of Supported Membrane Disruption by Antimicrobial Peptide Protegrin-1. *J. Phys. Chem. B* **2006**, *110*, 21282−21286.

(48) Debaisieux, S.; Rayne, F.; Yezid, H.; Beaumelle, B. The Ins and Outs of HIV-1 TAT. *Traffic* **2012**, *13*, 355−363.

(49) Wang, Y.; Agerberth, B.; Löthgren, A.; Almstedt, A.; Johansson, J. Apolipoprotein A-I Binds and Inhibits the Human Antibacterial/Cytotoxic Peptide LL-37. *J. Biol. Chem.* **1998**, *273*, 33115−33118.

(50) Sethi, A. A.; Stonik, J. A.; Thomas, F.; Demosky, S. J.; Amar, M.; Neufeld, E.; Brewer, H. B.; Davidson, W. S.; D'Souza, W.; Sviridov, D.; Remaley, A. T. Asymmetry in the Lipid Affinity of Bihelical Amphipathic Peptides: A Structural Determinant for the Specificity of ABCA1-Dependent Cholesterol Efflux by Peptides. *J. Biol. Chem.* **2008**, *283*, 32273−32282.

(51) Tanaka, M.; Takamura, Y.; Kawakami, T.; Aimoto, S.; Saito, H.; Mukai, T. Effect of Amino Acid Distribution of Amphipathic Helical Peptide Derived from Human Apolipoprotein A-I on Membrane Curvature Sensing. *FEBS Lett.* **2013**, *587*, 510−515.

(52) Segrest, J. P.; Chung, B. H.; Brouillette, C. G.; Kanellis, P.; McGahan, R. Studies of Synthetic Peptide Analogs of the Amphipathic Helix. Competitive Displacement of Exchangeable Apolipoproteins from Native Lipoproteins. *J. Biol. Chem.* **1983**, *258*, 2290−2295.

(53) Kingwell, B. A.; Chapman, M. J. Future of High-Density Lipoprotein Infusion Therapies. *Circulation* **2013**, *128*, 1112−1121.

(54) Murch, O.; Collin, M.; Hinds, C. J.; Thiemermann, C. Lipoproteins in Inflammation and Sepsis. I. Basic Science. *Intensive Care Med.* **2007**, *33*, 13−24.

(55) Jiao, Y.-l.; Wu, M.-P. Apolipoprotein A-I Diminishes Acute Lung Injury and Sepsis in Mice Induced by Lipoteichoic Acid. *Cytokine+* **2008**, *43*, 83−87.

(56) Zamanian-Daryoush, M.; Lindner, D.; Tallant, T. C.; Wang, Z.; Buffa, J.; Klipfell, E.; Parker, Y.; Hatala, D.; Parsons-Wingerter, P.; Rayman, P.; Yusufishaq, M. S. S.; Fisher, E. A.; Smith, J. D.; Finke, J.; DiDonato, J. A.; Hazen, S. L. The Cardioprotective Protein Apolipoprotein A1 Promotes Potent Anti-Tumorigenic Effects. *J. Biol. Chem.* **2013**, *288*, 21237−21252.

(57) De Nardo, D.; Labzin, L. I.; Kono, H.; Seki, R.; Schmidt, S. V.; Beyer, M.; Xu, D.; Zimmer, S.; Lahrmann, C.; Schildberg, F. A.; Vogelhuber, J.; Kraut, M.; Ulas, T.; Kerksiek, A.; Krebs, W.; Bode, N.; Grebe, A.; Fitzgerald, M. L.; Hernandez, N. J.; Williams, B. R. G.; et al. High-Density Lipoprotein Mediates Anti-Inflammatory Reprogramming of Macrophages *via* the Transcriptional Regulator ATF3. *Nat. Immunol.* **2014**, *15*, 152−160.

(58) Catapano, A. L.; Pirillo, A.; Bonacina, F.; Norata, G. D. HDL in Innate and Adaptive Immunity. *Cardiovasc. Res.* **2014**, *103*, 372−383.

(59) White, C. R.; Garber, D. W.; Anantharamaiah, G. M. Anti-Inflammatory and Cholesterol-Reducing Properties of Apolipoprotein Mimetics: A Review. *J. Lipid Res.* **2014**, *55*, 2007−2021.

(60) Remaley, A. T.; Amar, M.; Sviridov, D. HDL-Replacement Therapy: Mechanism of Action, Types of Agents and Potential Clinical Indications. *Expert Rev. Cardiovasc. Ther.* **2008**, *6*, 1203−1215.

(61) Buga, G. M.; Frank, J. S.; Mottino, G. A.; Hakhamian, A.; Narasimha, A.; Watson, A. D.; Yekta, B.; Navab, M.; Reddy, S. T.; Anantharamaiah, G. M.; Fogelman, A. M. D-4F Reduces EO6 Immunoreactivity, SREBP-1c mRNA Levels, and Renal Inflammation in LDL Receptor-Null Mice Fed a Western Diet. *J. Lipid Res.* **2008**, *49*, 192−205.

(62) McGrath, K. C.; Li, X.; Twigg, S. M.; Heather, A. K. Apolipoprotein-AI Mimetic Peptides D-4F and L-5F Decrease Hepatic Inflammation and Increase Insulin Sensitivity in C57BL/6 Mice. *PLoS One* **2020**, *15*, No. e0226931.

(63) Charles-Schoeman, C.; Banquerigo, M. L.; Hama, S.; Navab, M.; Park, G. S.; Van Lenten, B. J.; Wagner, A. C.; Fogelman, A. M.; Brahn, E. Treatment with an Apolipoprotein A-1 Mimetic Peptide in Combination with Pravastatin Inhibits Collagen-Induced Arthritis. *Clin. Immunol.* **2008**, *127*, 234−244.

(64) Yao, X.; Dai, C.; Fredriksson, K.; Dagur, P. K.; McCoy, J. P.; Qu, X.; Yu, Z.-X.; Keeran, K. J.; Zywicke, G. J.; Amar, M. J. A.; Remaley, A. T.; Levine, S. J. 5A, an Apolipoprotein A-I Mimetic Peptide, Attenuates the Induction of House Dust Mite-Induced Asthma. *J. Immunol.* **2011**, *186*, 576−583.

(65) Ditiatkovski, M.; Palsson, J.; Chin-Dusting, J.; Remaley, A. T.; Sviridov, D. Apolipoprotein A-I Mimetic Peptides. *Arterioscler., Thromb., Vasc. Biol.* **2017**, *37*, 1301−1306.

(66) Zhao, Y.; Imura, T.; Leman, L. J.; Curtiss, L. K.; Maryanoff, B. E.; Ghadiri, M. R. Mimicry of High-Density Lipoprotein: Functional Peptide−Lipid Nanoparticles Based on Multivalent Peptide Constructs. *J. Am. Chem. Soc.* **2013**, *135*, 13414−13424.

(67) Getz, G. S.; Wool, G. D.; Reardon, C. A. HDL Apolipoprotein-Related Peptides in the Treatment of Atherosclerosis and Other Inflammatory Disorders. *Curr. Pharm. Des.* **2010**, *16*, 3173−3184.

(68) Bloedon, L. T.; Dunbar, R.; Duffy, D.; Pinell-Salles, P.; Norris, R.; DeGroot, B. J.; Movva, R.; Navab, M.; Fogelman, A. M.; Rader, D. J. Safety, Pharmacokinetics, and Pharmacodynamics of Oral ApoA-I Mimetic Peptide D-4F in High-Risk Cardiovascular Patients. *J. Lipid Res.* **2008**, *49*, 1344−1352.